PAPER • OPEN ACCESS

Measurements of the cosmic-ray electron and positron spectrum and anisotropies with the Fermi LAT

To cite this article: F. Loparco and Fermi LAT Collaboration 2017 *J. Phys.: Conf. Ser.* **934** 012016

View the article online for updates and enhancements.

Measurements of the cosmic-ray electron and positron spectrum and anisotropies with the Fermi LAT

F. Loparco (on behalf of the Fermi LAT Collaboration)

Dipartimento di Fisica "M. Merlin" dell'Università e del Politecnico di Bari, I-70126 Bari, Italy
Istituto Nazionale di Fisica Nucleare, Sezione di Bari, I-70126 Bari, Italy

E-mail: `francesco.loparco@ba.infn.it`

Abstract. The Large Area Telescope (LAT) onboard the *Fermi* satellite is a pair-conversion telescope for high-energy gamma rays of astrophysical origin. Although it was designed to be a high-sensitivity gamma-ray telescope, the LAT has proved to be an excellent electron/positron detector. It has been operating in low Earth orbit since June 2008 and has collected more than 16 million cosmic-ray electron and positron (CRE) events in its first seven years of operation. The huge data sample collected by the LAT enables a precise measurement of the CRE energy spectrum up to the TeV region. A search for anisotropies in the arrival directions of CREs was also performed. The upper limits on the dipole anisotropy probe the presence of nearby young and middle-aged CRE sources.

1. Introduction
During their journey throughout the Galaxy, cosmic-ray electrons and positrons (CREs) rapidly lose energy by interacting through inverse Compton scattering with the interstellar radiation field and through synchrotron radiation with the Galactic magnetic field. The diffusion distances of CREs with energies above $100\,\mathrm{GeV}$ are of a few hundred pc, much shorter than the radius of the Galaxy, which is of the order of $10\,\mathrm{kpc}$. A combined measurement of the spectrum and of the anisotropies of high-energy CREs can, therefore, provide evidence for local CRE sources of astrophysical (supernova remnants and pulsar wind nebulae) or exotic (dark matter) nature.

2. The Fermi LAT as an electron/positron detector
The Large Area Telescope (LAT) is the main instrument onboard the *Fermi* satellite and is a pair-conversion telescope designed to detect gamma rays with energies above $20\,\mathrm{MeV}$. The LAT has a modular structure, consisting of 16 identical towers, each composed of a precision tracker-converter (TKR) and a calorimeter (CAL). The TKR consists of 18 x-y tracking planes of silicon strip detectors interleaved with tungsten converter foils, for a total on-axis thickness of 1.5 radiation lengths. The CAL consists of 96 CsI (Tl) crystals, hodoscopically arranged in 8 layers, for a total on-axis thickness if 8.6. radiation lengths. The towers are surrounded by a segmented anticoincidence detector (ACD) consisting of 89 plastic scintillators tiles, which is used for rejecting the charged cosmic-ray background. A full description of the LAT is given in ref. [1].
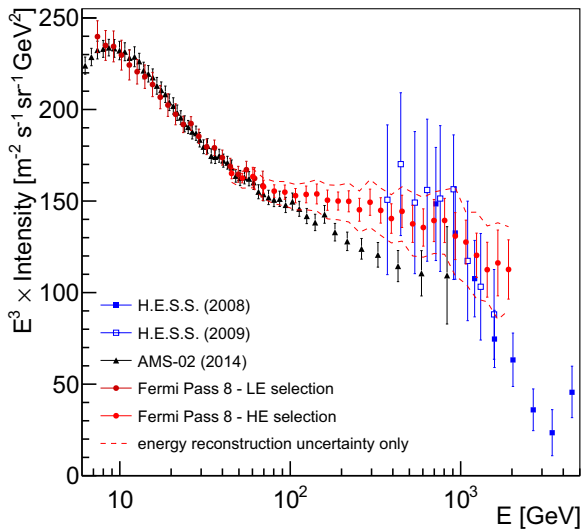
Figure 1. CRE spectrum measured by the *Fermi* LAT in its first seven years of operation. The results from the present analysis are compared with those from the AMS-02 [3] and H.E.S.S. [4, 5] experiments. The plot is taken from ref. [2].

Although it is designed to detect gamma rays, the LAT is able to collect and identify CREs with a large acceptance. In fact, like a gamma-ray, a CRE entering in the LAT will produce an electromagnetic shower which will start in the TKR and will develop in the CAL. The main difference between CRE and gamma-ray events resides in the response of the ACD: while in a gamma-ray event no signal is expected from the ACD tile intersected by the shower axis (since gamma-ray conversion must take place in the TKR), in a CRE event a signal from a singly-charged particle is expected.

The LAT trigger system takes inputs from the ACD, TKR and CAL detectors. After an event passes the hardware trigger, it is inspected by the onboard software filters, that are configured to identify events likely to be useful for scientific or calibration purposes. Four onboard filters are implemented:

- Gamma filter, designed to select gamma-ray candidates and events that deposit at least 20 GeV in the CAL;

- Heavy-ion filter, designed to perform calibrations on high energy scales;

- MIP filter, designed to select minimum ionizing charged particles;

- Diagnostic filter, designed to select an unbiased event sample for filter performance and background studies. Events selected by this filter are prescaled of a factor 250.

If an event is accepted by any filter, all its information is recorded and transmitted to the ground.

Two independent CRE analyses have been implemented: the high-energy (HE) analysis, above 42 GeV, which uses a sample of events passing the onboard gamma filter, and the low-energy (LE) analysis between 7 and 70 GeV, which uses a sample of events passing the diagnostic filter. In both cases, we first apply a set of preliminary cuts before performing a multivariate analysis in order to reduce the residual proton contamination as much as possible. For both the HE and the LE analyses, these cuts are combined with further selections based on multivariate classification analyses. A full description of the analysis is given in ref. [2].

3. The CRE energy spectrum
For the present analysis, we have used a sample of Pass 8 data collected by the LAT between August 4, 2008, and June 24, 2015. The overall live time for this data set is 4.68 years. In Fig. 1 the measured CRE spectrum is shown and is compared with the previous measurements

performed by the AMS-02 [3] and by the H.E.S.S. [4, 5] experiments. The results from the HE and from the LE analyses match very well over the overlapping range from $42\,\text{GeV}$ to $70\,\text{GeV}$.

The LAT results are in good agreement with the AMS-02 data up to about $200\,\text{GeV}$, while in the region above $400\,\text{GeV}$ they are consistent with the H.E.S.S. data. The spectrum is well fitted by a broken power law, with a break energy of $(53\pm8)\,\text{GeV}$ and spectral indices 3.21 ± 0.02 and 3.07 ± 0.02 below and above the break respectively.

The H.E.S.S. data above $600\,\text{GeV}$ reported in [4] are well reproduced by an exponentially cutoff power law with an index of 3.05 ± 0.02 and a cutoff at $2.1\pm0.3\,\text{TeV}$. The LAT CRE spectrum above $50\,\text{GeV}$ is compatible with a single power law with a spectral index of 3.07. A fit of the spectrum above $50\,\text{GeV}$ with an exponentially cutoff power law does not yield statistically significant evidence for a cutoff below $1.8\,\text{TeV}$ at 95% confidence level.

4. Search for anisotropies in the CRE arrival directions

The search for possible anisotropies in the CRE arrival directions has been performed using the HE sample in the range from $42\,\text{GeV}$ to $2\,\text{TeV}$. The energy interval has been divided in 9 bins. To reduce geomagnetic effects (which could mimic a true anisotropy signal), we have performed the analysis with a reduced field of view. In particular, for each energy bin, we have set an allowed maximum off-axis angle θ_{max} ($40°$ for $42\,\text{GeV} < E < 56\,\text{GeV}$, $50°$ for $56\,\text{GeV} < E < 75\,\text{GeV}$ and $60°$ for $E > 75\,\text{GeV}$). In this way particles with large zenith angles, which might be affected by the geomagnetic field, have been discarded.

The strategy to search for possible anisotropies is to compare the observed sky maps in each energy bin with the corresponding reference maps that should be seen by the instrument if the CRE flux was isotropic, and represent the null hypothesis.

The starting point of the analysis is therefore the construction of the reference (isotropic) sky maps. Since the expected signal is tiny, in order to mitigate potential systematic uncertainties arising from the calculation of the detector exposure, we have built the reference maps using four different data-driven methods. The first method ("shuffling technique") consists of generating a set of simulated events starting from the real event sample and randomly associating detected event times and instrument angles. The sky direction of a simulated event is built combining the position and orientation of the LAT at the time of the i-th event with the angles in the LAT frame taken from the the j-th event, where (i, j) are two random numbers in the interval $[1, N]$ (N is the total number of observed events). In the second method ("event rate technique"), each simulated event is assigned a time generated from an exponential distribution with the same average rate as in the real data, and a direction in the LAT frame generated from the observed distribution $P(\theta, \phi)$. The other two methods combine the previous techniques, i.e. one can extract the event times sequence from an exponential distribution with given average rate and take the angles (θ, ϕ) from real events, or one can take the observed times from real events and draw the angles from the distribution $P(\theta, \phi)$. All these methods have been validated with dedicated Monte Carlo simulations [6].

Several methods have been implemented to compare the observed sky maps with the reference ones. The first option is to implement a direct pixel-to-pixel comparison. However, a more powerful approach is that of applying this method to integrated sky maps, in which each pixel contains the integrated number of events in a given circular region of fixed angular radius around the pixel itself. This approach increases the sensitivity to possible anisotropies with the same angular scale as the integration radius. Finally, another strategy is the spherical harmonic analysis of a fluctuation sky map. The fluctuation in each pixel is defined as $f_i = (n_i - \mu_i)/\mu_i$, where n_i and μ_i are the events of the real and of the reference map in the i-th pixel. The fluctuations map is expanded in the basis of spherical harmonics, producing a set of coefficients a_{lm}, which are used to build the multipole coefficients $\hat{C}_l$ of the angular power spectrum (APS). Each multipole coefficient is sensitive to anisotropies at an angular scale $180°/l$.
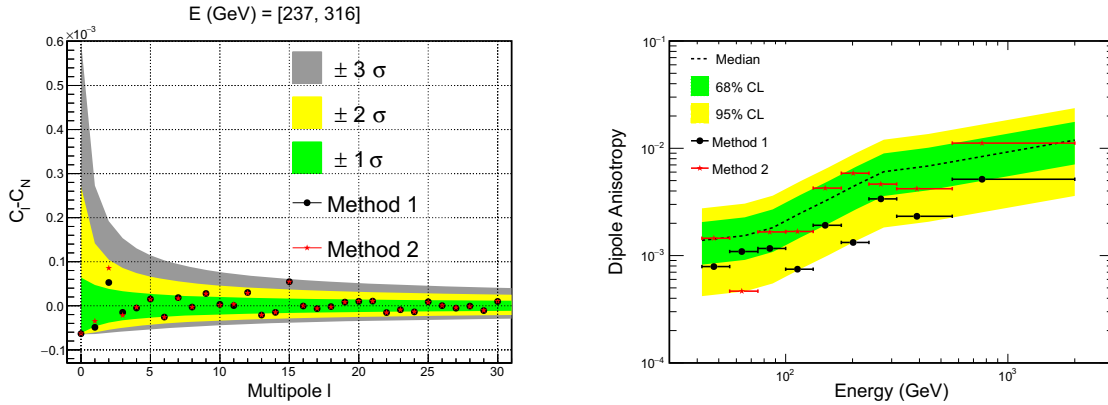
Figure 2. Left panel: measured APS in the energy bin from $237\,\mathrm{GeV}$ to $316\,\mathrm{GeV}$. The difference $C_l - C_N$ is plotted as a function of the multipole l. Right panel: measured dipole anisotropy as a function of energy. The colored bands in both plots represent the expected central confidence intervals for an isotropic sky. The plots are taken from ref. [6].

Each multipole coefficient C_l can be viewed as a sum of two terms, i.e. $\hat{C}_l = C_N + \hat{C}_l^{ani}$, where C_N is the Poisson (white) noise term due to the finite number of events in the map, while $\hat{C}_l^{ani}$ is the anisotropy term. If the sky is observed with non-uniform exposure, the white noise is given by $C_N = \left(4\pi/N_{pixels}^2\right)\sum_i n_i/\mu_i^2$ where N_{pixels} is the number of pixels in the map [7]. To check whether the observed APS is statistically compatible with the Poisson noise, we have tested the null hypothesis $\hat{C}_l = C_N$ against the alternative hypothesis $\hat{C}_l > C_N$. The left plot of Fig. 2 shows an example of APS evaluated in the energy bin from $237\,\mathrm{GeV}$ to $316\,\mathrm{GeV}$. The data lie within the expectation bands obtained assuming the null hypothesis. The same behavior is observed in all the energy bins.

The first multipole coefficient is directly related to the dipole anisotropy coefficient, which is given by $\delta = 3\sqrt{C_1/4\pi}$. The right plot of Fig. 2 shows the measured values of δ as a function of energy. The measured values are consistent with the expectations obtained assuming the null hypothesis. We can, therefore, conclude that no anisotropies are observed in the CRE data, and we can set upper limits on the value of the dipole anisotropy coefficient.

5. Discussion and conclusions

The measured CRE spectrum and anisotropies can be compared with the predictions from various astrophysical models. We have tested a model in which CREs arriving in the Solar System consists of a galactic diffuse component and of an additional component originated from a local nearby source.

To evaluate the spectrum of the galactic CRE component we have used the two-dimensional version of the DRAGON propagation code [8] with the secondary particle production cross sections of ref. [9], assuming that the scalar diffusion coefficient depends on the particle rigidity R and on the distance from the galactic plane z according to the parametrization $D = D_0(R/R_0)^{0.33}e^{|z|/z_t}$, where $D_0 = 4.25 \times 10^{28}\,\mathrm{cm^2 s^{-1}}$, $R_0 = 4\,\mathrm{GV}$ and $z_t = 4\,\mathrm{kpc}$. The Alfvén velocity is set to $v_A = 33\,\mathrm{km\ s^{-1}}$

We have then considered the contributions from two possible sources located either in the Vela (distance $290\,\mathrm{pc}$, age $1.1 \times 10^4\,\mathrm{yrs}$) or in the Monogem (distance $290\,\mathrm{pc}$, age $1.1 \times 10^5\,\mathrm{yrs}$) positions. For both sources, we have adopted a burst like electron injection spectrum, in which the duration of the emission is much shorter than the travel time from the source, described by a
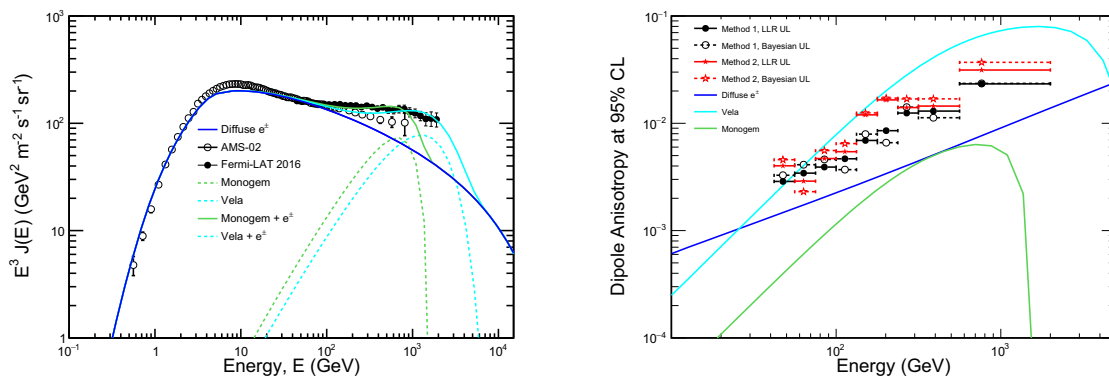
Figure 3. Left panel: CRE spectra measured by the *Fermi* LAT and AMS02 [3]. The blue line represents the galactic CRE contribution evaluated with DRAGON [8, 9]. The green (cyan) lines represent the contribution from Monogem (Vela) alone (dashed lines) and the sum of the Monogem (Vela) contribution with the galactic component (solid lines). Right panel: upper limits on the dipole anisotropy measured by the LAT compared with the predictions obtained assuming a CRE source in the Monogem (green line) or in the Vela (cyan line) position. The plots are taken from ref. [6].

power law with index $\Gamma = 1.7$ and with an exponential cutoff $E_{\text{cut}} = 1.1\,\text{TeV}$. For both sources, the normalization of the spectrum has been chosen to obtain a total flux not higher than that measured by the *Fermi* LAT and by AMS02 [3]. The left panel of Fig. 3 shows the CRE spectra measured by the *Fermi* LAT and by AMS02 compared with those predicted by the model.

In the right panel the upper limits on the CRE dipole anisotropy obtained by the LAT are compared with the predictions of the model. The LAT limits are consistent with the expected anisotropy in a scenario with a nearby middle-aged CRE source (Monogem), but are lower than the expected anisotropy in a scenario with a nearby young CRE source (Vela).

References

[1] Atwood W B *et al.* 2009 *Astrophys. J.* **697** 1071
[2] Abdollahi S *et al.* 2017 *Phys. Rev.* D **95** 082007
[3] Aguilar M *et al.* 2014 *Phys. Rev. Lett.* **113** 221102
[4] Aharonian F *et al.* 2008 *Phys. Rev. Lett.* **101** 261104
[5] Aharonian F *et al.* 2009 *Astron. & Astrophys.* **508** 561
[6] Abdollahi S *et al.* 2017 *Phys. Rev. Lett.* **118** 091103
[7] Fornasa M *et al.* 2016 *Phys. Rev.* D **94** 123005
[8] Evoli C *et al.* 2008 *J. Cosmol. Astropart. Phys.* **10** 018
[9] Mazziotta M N *et al.* 2016 *Astrop. Phys.* **81** 21